American Mineralogist, Volume 60, pages 423–434, 1975

The Effect of Ca-Fe Substitution on the Clinopyroxene Crystal Structure

YOSHIKAZU OHASHI,

Geophysical Laboratory, Carnegie Institution of Washington, Washington, D. C. 20008

CHARLES W. BURNHAM,

Department of Geological Sciences, Harvard University, Cambridge, Massachusetts 02138

AND LARRY W. FINGER

Geophysical Laboratory, Carnegie Institution of Washington, Washington, D. C. 20008

Abstract

The major structural change resulting from Ca-Fe substitution in four clinopyroxenes of intermediate composition between hedenbergite and ferrosilite, measured at room temperature, is in the size and shape of the $M2$ polyhedron, whereas the $M1$ polyhedron remains essentially unchanged. The decrease in the average size of the $M2$ polyhedron associated with a compositional change from hedenbergite to ferrosilite causes kinking of the tetrahedral chain and concomitant increases in the out-of-plane tilting of the basal face of the tetrahedron. As the $M2$ polyhedron decreases further in size, the space group changes from $C2/c$ to $P2_1/c$ at about $Fs_{80}Wo_{20}$ composition. When the composition changes from $Fs_{85}Wo_{15}$ to $Fs_{100}Wo_0$, the A chain extends and finally reverses its kink direction. The anisotropic temperature factors for these intermediate compositions may be explained as a result of the effects of positional disorder.

Introduction

Most minerals can form solid solutions, either limited or complete, and thus some sites in the unit cells of minerals are occupied statistically by more than one atomic species. If there is a large difference in the ionic radii of the atoms occupying the site, the crystal structure may change with a change in occupancy of the site and thus in the apparent size of the coordination polyhedron. One of the best mineralogical examples of multiple occupancy is augite-pigeonite, where substitution of Ca for Fe or Mg is involved.

In the pyroxene quadrilateral (diopside-enstatite-ferrosilite-hedenbergite system) the clinopyroxene space groups are $P2_1/c$ for Ca-poor (pigeonite) compositions and $C2/c$ for Ca-rich (augite) compositions at room temperature. The major differences between the $P2_1/c$ and $C2/c$ structures are that (1) there is only one crystallographically distinct silicate chain in the $C2/c$ structure, whereas two types of the chains exist in the $P2_1/c$ structure, and (2) the $M2$ site[1] is eight-coordinated in the $C2/c$ end members (diopside: Clark, Appleman, and Papike, 1969; hedenbergite: Veblen, 1969, and Cameron *et al,* 1973) and six-coordinated in the $P2_1/c$ end members (clinoferrosilite: Burnham, 1967; clinoenstatite: Morimoto, Appleman, and Evans, 1960).

In clinopyroxenes of intermediate composition, the $M2$ site is very irregular as a result of multiple occupancy of the large Ca and small Fe or Mg atoms in the site. In a structural refinement of a pigeonite, $Mg_{0.39}Fe_{0.52}Ca_{0.09}SiO_3$ from Mull, Scotland, Morimoto and Güven (1970) reported a very irregular $M2$ coordination polyhedron, which they concluded was an average of eight and six coordinations. Güven (1969) studied the relationship between the average size of $M2$ and kinking of the

[1] Nomenclature for the pyroxenes is that proposed by Burnham *et al* (1967).

tetrahedral chain. Takeda (1972) discussed variation of $M2$–O bonds in clinopyroxenes as a function of Ca content and showed that the $M2$ polyhedron becomes very irregular, thus highly unstable, in the middle of the solid solution. He proposed that irregularity of the $M2$ polyhedral shape provided a structural explanation for the presence of a miscibility gap. In their crystal structural study of six end-member clinopyroxenes at high temperatures, Cameron *et al* (1973) explained the increased solid solution between the Ca-poor and Ca-rich clinopyroxenes at high temperature by the change in $M2$ coordination associated with the $P2_1/c$–$C2/c$ phase transition.

The present study is concerned primarily with the effects of chemical substitution on the structure studied at room temperature. To eliminate the structural effects of possible changes of Mg-Fe distribution in the cation sites, the binary join hedenbergite ($CaFeSi_2O_6$)–clinoferrosilite ($Fe_2Si_2O_6$) was selected. Therefore, these structures reflect solely a difference between Ca and Fe contents. Furthermore, if the $M1$ site on the join studied is occupied only by Fe atoms, as expected from its polyhedral size, it is possible to isolate the effects of changes of the $M2$ site on the other parts of the structure, especially the tetrahedral chain configuration.

Experimental

Unit Cell and Space Group

Synthetic single crystals of clinopyroxenes on the hedenbergite–clinoferrosilite join were kindly supplied by Dr. D. H. Lindsley. Synthesis techniques were described by Lindsley and Munoz (1969, Appendix). Crystals of $Fs_{85}Wo_{15}$,[2] $Fs_{80}Wo_{20}$, $Fs_{75}Wo_{25}$ (all synthesized at 20 kbar and 950°C), and $Fs_{65}Wo_{35}$ (6 kbar and 1140°C) have been examined using the Buerger precession camera. Class b reflections ($h + k$ = odd) are exhibited by $Fs_{85}Wo_{15}$ and some crystals of $Fs_{80}Wo_{20}$, whereas long-exposure photographs of $Fs_{65}Wo_{35}$, $Fs_{70}Wo_{30}$, and the other crystals of $Fs_{80}Wo_{20}$ do not show these b reflections. Thus the (metastable) boundary at room temperature between the space groups $P2_1/c$ and $C2/c$ is close to the $Fs_{80}Wo_{20}$ composition on the join hedenbergite–ferrosilite. At low pressures the clinopyroxene of this composition is not stable relative to the assemblage fayalite + tridymite (Bowen, Schairer, and Posnjak, 1933; Lindsley and Munoz, 1969). No exsolved phases are detected on long-exposure precession photographs, and thus the crystals are considered to be homogeneous.

TABLE 1. Unit-Cell Parameters and Unit-Cell Volume of Ca-Fe Clinopyroxenes

	$Fs_{65}Wo_{35}$	$Fs_{75}Wo_{25}$	$Fs_{80}Wo_{20}$	$Fs_{85}Wo_{15}$
a (Å)	9.812(1)*	9.781(2)	9.760(6)	9.779(1)
b (Å)	9.049(1)	9.072(2)	9.057(8)	9.088(1)
c (Å)	5.233(1)	5.246(2)	5.234(3)	5.258(1)
β (deg.)	105.34(1)	106.55(2)	106.28(5)	107.39(1)
V (Å^3)	448.1(1)	446.2(3)	444.1(6)	445.9(2)
Method**	BW	BW	FD	BW

*Parenthesized figures represent the estimated standard deviation (esd) in terms of least units cited for the value to their immediate left, thus for 9.812(1) read 9.812 ± 0.001.
**BW: back-reflection Weissenberg camera.
FD: four-circle diffractometer.

Unit-cell parameters of crystals other than $Fs_{80}Wo_{20}$ were measured using a back-reflection precision Weissenberg camera. Data for both Cu$K\alpha_1$ and $K\alpha_2$ wavelengths were refined by the least-squares method and included corrections for film shrinkage, camera eccentricity, and specimen absorption (Burnham, 1962). Unit-cell parameters for $Fs_{80}Wo_{20}$ were determined by a lattice-constant refinement subroutine for a four-circle diffractometer. This subroutine, which is a part of the Geophysical Laboratory diffractometer system, has some new features: auto-centering of reflections and least-squares refinement of the orientation matrix from which the unit-cell parameters (Table 1) are calculated (Finger, unpublished; Gabe, Alexander, and Goodman, 1970). Analysis of the clinopyroxene lattice deformation due to chemical substitution on this join is given elsewhere (Ohashi and Burnham, 1973).

Measurement and Reduction of X-Ray Intensity Data

Intensity data were collected using a computer-controlled Picker four-circle diffractometer with Nb-filtered Mo$K\alpha$ radiation. Reflections in one quadrant of reciprocal space within the range 0.1 to 0.8 of sin θ/λ were measured employing ω-2θ scans. The observed intensities were corrected for Lorentz and polarization effects and for absorption using the numerical integration techniques of Burnham (1966). In addition, the secondary extinction factor of Zachariasen (1968) was calculated for the $Fs_{75}Wo_{25}$ and $Fs_{80}Wo_{20}$ crystals.

The crystal of $Fs_{85}Wo_{15}$ is twinned on (100). Therefore, the $hk0$ reflections contain superimposed contributions from both twin components. By com-

[2] Compositions are in molecular proportions of Fs ($FeSiO_3$) and Wo ($CaSiO_3$). Crystals of $Fs_{65}Wo_{35}$ and $Fs_{75}Wo_{25}$ were examined using the electron microprobe. No inhomogeneities were observed with the error in composition estimated to be less than 3 mole percent Fs.

TABLE 2. Crystal and Refinement Data for Ca-Fe Clinopyroxenes

	$Fs_{65}Wo_{35}$	$Fs_{75}Wo_{25}$	$Fs_{80}Wo_{20}$	$Fs_{85}Wo_{15}$
Space group	C2/c	C2/c	C2/c	$P2_1/c$
Size of crystal (mm)	0.13x0.20 x0.39	0.03x0.04 x0.21	0.09x0.11 x0.14	0.07x0.08 x0.29
Linear absorption coefficient (cm^{-1}) for MoKα	56.28	60.74	63.14	64.98
Range of transmission factor (%)	31-56	78-85	57-67	60-70
Number of reflections used in refinement	967	492	785	1144
Residual factor (%)*				
R	4.3	5.8	4.9	6.2
R(wtd.)	3.7	5.5	5.3	4.2

*$R = \Sigma||F_o| - |F_c||/\Sigma|F_o|$.

$R(wtd.) = [\Sigma w(|F_o| - |F_c|)^2/\Sigma w|F_o|^2]^{1/2}$.

paring the intensities of the two twin components for several *hkl* reflections that were resolved, the volume of one component was estimated as 95.4 percent of the crystal volume, and the proper correction was made for the unresolved *hk*0 reflections.

TABLE 3. Atomic Positional Parameters and Equivalent Isotropic Temperature Factors for Ca-Fe Clinopyroxenes*

		$Fs_{65}Wo_{35}$ (C2/c)	$Fs_{75}Wo_{25}$ (C2/c)	$Fs_{80}Wo_{20}$ (C2/c)	$Fs_{85}Wo_{15}$ ($P2_1/c$)	
					A chain	B chain
M1 (Fe)	x	0	0	0	0.2512(2)	
	y	0.9064(1)†	0.9047(3)	0.9050(1)	0.6543(1)	
	z	1/4	1/4	1/4	0.2454(4)	
	$B_{eq.}$**	0.44(1)	0.80(4)	0.64(2)	0.67(1)	
M2	Ca occ.††	0.7	0.5	0.4	0.3	
	Fe occ.	0.3	0.5	0.6	0.7	
	x	0	0	0	0.2534(3)	
	y	0.2908(1)	0.2747(3)	0.2751(1)	0.0182(1)	
	z	1/4	1/4	1/4	0.2443(5)	
	$B_{eq.}$	1.31(2)	1.85(6)	1.78(3)	1.46(2)	
Si	x	0.2901(1)	0.2936(2)	0.2937(1)	0.0461(3)	0.5455(3)
	y	0.0910(1)	0.0898(3)	0.0891(1)	0.3387(4)	0.8373(4)
	z	0.2370(1)	0.2434(4)	0.2440(2)	0.2569(5)	0.2436(5)
	$B_{eq.}$	0.41(1)	0.75(4)	0.65(2)	0.73(4)	0.63(4)
O1	x	0.1207(2)	0.1207(6)	0.1214(3)	0.8729(6)	0.3719(7)
	y	0.0895(3)	0.0893(8)	0.0893(3)	0.3407(10)	0.8360(12)
	z	0.1526(4)	0.1517(11)	0.1535(6)	0.1601(12)	0.1499(14)
	$B_{eq.}$	0.63(3)	0.82(8)	0.78(4)	0.60(9)	0.95(11)
O2	x	0.3658(3)	0.3706(7)	0.3712(4)	0.1182(9)	0.6280(7)
	y	0.2448(3)	0.2426(7)	0.2417(3)	0.4948(11)	0.9873(9)
	z	0.3317(5)	0.3496(16)	0.3480(8)	0.3423(17)	0.3656(16)
	$B_{eq.}$	1.10(4)	1.75(14)	1.53(6)	1.71(14)	0.99(12)
O3	x	0.3505(2)	0.3520(7)	0.3517(3)	0.1002(7)	0.6038(8)
	y	0.0222(2)	0.0255(7)	0.0261(4)	0.2299(10)	0.7192(9)
	z	-0.0055(4)	-0.0043(14)	-0.0020(6)	0.5172(14)	0.4983(13)
	$B_{eq.}$	0.70(3)	1.26(10)	1.14(5)	1.95(15)	1.13(12)

*Fractional coordinates refer to the conventional origin in those space groups. Coordinate translations between two origins are $x_p = x_c \pm 1/4$, $y_p = y_c \pm 1/4$, and $z_p = z_c$.

**$B_{eq.}$ = Equivalent isotropic temperature factor computed from anisotropic temperature factors, β_{ij}, according to $B_{eq.} = \frac{4}{3}\Sigma\Sigma\beta_{ij}\,\underline{a}_i \cdot \underline{a}_j$ (Hamilton, 1959).

†Parenthesized figures represent the estimated standard deviation (esd) in terms of least units cited for the value to their immediate left, thus for 0.9064(1) read 0.9064 ± 0.0001.

††Occupancy of the M2 site is fixed by bulk chemical composition (see text).

Refinement Procedures

Throughout all refinements, the least-squares program RFINE of Finger was used on the IBM 370 and the UNIVAC 1108 computers. Atomic scattering factors were those of Fe^{2+}, Ca^{2+}, Si^{4+}, and O^- given by Cromer and Mann (1968) with the anomalous dispersion coefficients of Cromer (1965).

Least-squares refinements of $Fs_{65}Wo_{35}$ and $Fs_{85}Wo_{15}$ were initiated with atomic parameters of hedenbergite (Veblen, 1969) and clinoferrosilite (Burnham, 1967), respectively. Refined parameters of $Fs_{65}Wo_{35}$ and $Fs_{75}Wo_{25}$, respectively, were used as initial parameters of $Fs_{75}Wo_{25}$ and $Fs_{80}Wo_{20}$. Reflections were weighted according to $w = 1/\sigma^2$, where σ is the estimated standard deviation of the observed structure factor. Reflections were rejected from least-squares refinement if the intensity was below two standard deviations of the observed intensity based on counting statistics. At the later stage of least-squares refinement, reflections with $\Delta F = F_o - F_c$ greater than 6 were also rejected.

In each structure the atomic positions, anisotropic temperature factor coefficient, and a scale factor were refined. In addition, the isotropic extinction parameter of Zachariasen (1968) was refined for the $Fs_{75}Wo_{25}$ and $Fs_{80}Wo_{20}$ data sets. The correction for the twinning in $Fs_{85}Wo_{15}$ was tested by refining a separate scale factor for (*hk*0). The resulting values were essentially identical, confirming the validity of the prior correction. No strong correlations between parameters were found for the $C2/c$ structural refinements. However, the *A* and *B* chains in the $P2_1/c$ structure are in general highly correlated: −0.75 between β_{12}'s of Si*A* and Si*B* and −0.71 between *y*'s of O1*A* and O1*B* were found to be the strongest correlations.

From an ionic size consideration, all Ca atoms are assumed to occupy the larger *M*2 site. Thus, for example, the occupancy of cation sites for $Fs_{85}Wo_{15}$ is 100 percent Fe^{2+} in the *M*1 site and (70 percent Fe^{2+} + 30 percent Ca) in the *M*2 site.

Data for the crystals and refinements are summarized in Table 2. The final positional parameters and temperature factors are given in Tables 3 and 4, respectively. Tables of observed and calculated structure factors may be ordered.[3]

[3] To receive a copy of these structure factor tables, order document AM-75-001 from the Business Office, Mineralogical Society of America, suite 1000 lower level, 1909 K Street, N.W., Washington, D. C. 20006. Please remit $1.00 for the microfiche.

TABLE 4. Anisotropic Temperature Factors for Ca-Fe Clinopyroxenes*

		$Fs_{65}Wo_{35}$	$Fs_{75}Wo_{25}$	$Fs_{80}Wo_{20}$	$Fs_{85}Wo_{15}$	
					A chain	B chain
M1	β_{11}	0.0017(1)**	0.0019(2)	0.0017(1)	0.0018(1)	
	β_{22}	0.0010(1)	0.0024(2)	0.0015(1)	0.0022(1)	
	β_{33}	0.0038(2)	0.0091(8)	0.0093(3)	0.0067(3)	
	β_{12}	0	0	0	0.0002(2)	
	β_{13}	0.0008(1)	0.0012(3)	0.0022(1)	0.0012(1)	
	β_{23}	0	0	0	0.0002(4)	
M2	β_{11}	0.0025(1)	0.0026(3)	0.0022(1)	0.0020(1)	
	β_{22}	0.0074(1)	0.0100(4)	0.0105(2)	0.0082(1)	
	β_{33}	0.0050(3)	0.0105(11)	0.0105(4)	0.0079(3)	
	β_{12}	0	0	0	-0.0001(2)	
	β_{13}	0.0001(1)	-0.0007(4)	0.0010(2)	-0.0001(1)	
	β_{23}	0	0	0	0.0007(4)	
Si	β_{11}	0.0014(1)	0.0018(2)	0.0015(1)	0.0012(2)	0.0021(2)
	β_{22}	0.0012(1)	0.0019(2)	0.0016(1)	0.0028(3)	0.0014(3)
	β_{33}	0.0038(2)	0.0103(9)	0.0106(4)	0.0083(7)	0.0078(7)
	β_{12}	-0.0002(1)	-0.0001(3)	-0.0003(1)	0.0003(3)	-0.0007(3)
	β_{13}	0.0011(1)	0.0019(3)	0.0028(1)	0.0009(3)	0.0020(4)
	β_{23}	-0.0005(1)	-0.0000(6)	-0.0008(2)	-0.0008(5)	-0.0007(5)
O1	β_{11}	0.0021(2)	0.0020(5)	0.0016(2)	0.0013(5)	0.0023(7)
	β_{22}	0.0018(2)	0.0023(5)	0.0024(3)	0.0021(7)	0.0035(8)
	β_{33}	0.0056(7)	0.0113(23)	0.0106(10)	0.0048(18)	0.0103(23)
	β_{12}	0.0003(2)	0.0001(7)	0.0002(2)	-0.0000(7)	0.0000(8)
	β_{13}	0.0011(3)	0.0024(9)	0.0019(4)	-0.0008(8)	0.0026(11)
	β_{23}	0.0002(4)	-0.0025(15)	0.0000(5)	0.0002(13)	-0.0010(16)
O2	β_{11}	0.0039(2)	0.0036(7)	0.0043(3)	0.0055(8)	0.0017(6)†
	β_{22}	0.0023(2)	0.0024(7)	0.0025(3)	0.0041(9)	0.0017(8)
	β_{33}	0.0134(9)	0.0355(42)	0.0287(16)	0.0232(33)	0.0192(28)
	β_{12}	-0.0013(2)	-0.0006(6)	-0.0018(3)	0.0001(8)	-0.0019(6)
	β_{13}	0.0039(4)	0.0070(14)	0.0088(6)	0.0076(14)	0.0027(11)
	β_{23}	-0.0022(4)	-0.0012(15)	-0.0040(6)	-0.0005(15)	-0.0035(13)
O3	β_{11}	0.0018(2)	0.0021(5)	0.0018(3)	0.0006(6)	0.0026(8)
	β_{22}	0.0030(2)	0.0058(7)	0.0053(4)	0.0106(12)	0.0056(9)
	β_{33}	0.0049(7)	0.0111(22)	0.0120(11)	0.0193(25)	0.0098(22)
	β_{12}	-0.0000(2)	0.0007(6)	-0.0001(3)	0.0012(6)	-0.0007(6)
	β_{13}	0.0008(3)	0.0013(9)	0.0029(4)	0.0001(11)	0.0041(11)
	β_{23}	-0.0014(4)	-0.0029(13)	-0.0032(5)	0.0105(14)	0.0015(11)

*Anisotropic temperature factors, β_{ij}, are in the form of

$$\exp - \{\beta_{11}h^2 + \beta_{22}k^2 + \beta_{33}\ell^2 + 2\beta_{12}hk + 2\beta_{13}h\ell + 2\beta_{23}k\ell\}$$

**Parenthesized figures represent the estimated standard deviation (esd) in terms of least units cited for the value to their immediate left, thus for 0.0017(1) read 0.0017 ± 0.0001.

Results and Discussion

M1 and M2 Sites

Interatomic distances for the *M*1 and *M*2 sites are given in Table 5. The *M*1–O bond distances (Fig. 1) and the polyhedral volume (Table 5) both show essentially no change for the *M*1 site with Ca-Fe substitution. This observation seems to verify the assumption that all calcium is restricted to *M*2 on the join studied. As characterized by the quadratic elongation and the angle variance given in Table 5 (quantities proposed by Robinson, Gibbs, and Ribbe, 1971, as measures of polyhedral distortion), the *M*1 polyhedron deviates slightly more from an ideal octahedron on the Fe-rich side. It is, however, still much more regular than the *M*2 polyhedron (quadratic elongation = 1.06 and angle variance = 164° for *M*2 in clinoferrosilite).

The *M*2 site changes from eight-coordinated in hedenbergite to six-coordinated in ferrosilite. Details of this change are one of the main points of interest in the present study. With increasing Fe content, the *M*2 polyhedral volume decreases and the *M*2–O1 and *M*2–O2 distances also decrease (Fig. 1), as a result of substitution of smaller Fe atoms for larger Ca atoms. On the other hand, all four *M*2–O3 distances increase when the composition changes from $Fs_{50}Wo_{50}$ to $Fs_{80}Wo_{20}$. In the $P2_1/c$ region these bonds split into two groups, one increasing and the other decreasing with further Fe enrichment. In clinoferrosilite only six *M*2–O distances are less than 3 Å, the approximate value of the shortest oxygen-oxygen or metal-metal distance.

This change of the *M*2 coordination can be visualized with the aid of Figure 2. The changes of the *M*2–O distances occur as a consequence of a rotation of the O3*A*1–O3*A*2 and O3*B*1–O3*B*2 vectors in

TABLE 5. Interatomic Distances *M*1–O and *M*2–O in Ca-Fe Clinopyroxenes

		$Fs_{65}Wo_{35}$	$Fs_{75}Wo_{25}$	$Fs_{80}Wo_{20}$	$Fs_{85}Wo_{15}$
	M1 Site				
1	M1–O1A1	2.127(2)*	2.103(6)	2.113(3)	2.116(7)
2	–O1B2				2.103(8)
3	–O1A2	2.175(2)	2.192(7)	2.187(3)	2.225(8)
4	–O1B1				2.174(9)
5	–O2A	2.086(2)	2.101(7)	2.096(3)	2.109(9)
6	–O2B				2.110(8)
Mean		2.129	2.132	2.132	2.140
Quad. Elong.**		1.0042	1.0057	1.0053	1.0065
Ang. Var. (deg.^{2})**		13.5	17.7	16.9	20.4
Polyhedral Volume (Å^3)		12.8	12.8	12.8	12.9
	M2 Site				
1	M2–O1A	2.302(2)	2.198(6)	2.197(3)	2.179(8)
2	–O1B				2.162(9)
3	–O2A	2.259(3)	2.127(8)	2.133(4)	2.135(10)
4	–O2B				2.033(9)
5	–O3A1	2.765(2)	2.844(8)	2.842(4)	2.800(9)
6	–O3B2				2.889(8)
7	–O3A2	2.700(2)	2.822(7)	2.817(4)	3.048(8)
8	–O3B1				2.825(7)
Mean of 4, Nbr†		2.281	2.163	2.165	2.127
Mean of 4, Br†		2.733	2.833	2.830	2.891
Mean of 8		2.507	2.498	2.497	2.509
Polyhedral Volume (Å^3)		25.7	24.7	24.7	24.8 [8-coord.] 18.1 [7-coord.]

*Parenthesized figures represent the estimated standard deviation (esd) in terms of least units cited for the value to their immediate left, thus for 2.127(2) read 2.127 ± 0.002.

**Octahedral quadratic elongation (Robinson et al., 1971) defined by $\sum_{i=1}^{6} (\ell_i/\ell_o)^2/6$, where ℓ_o is the center-to-vertex distance for an ideal octahedron whose volume is equal to that of the observed M1 octahedron.

Octahedral angle variance defined by $\sum_{i=1}^{12} (\theta_i - 90)^2/11$.

†Nbr: nonbridging oxygen atoms (O1 and O2) and
Br: bridging oxygen atom (O3).

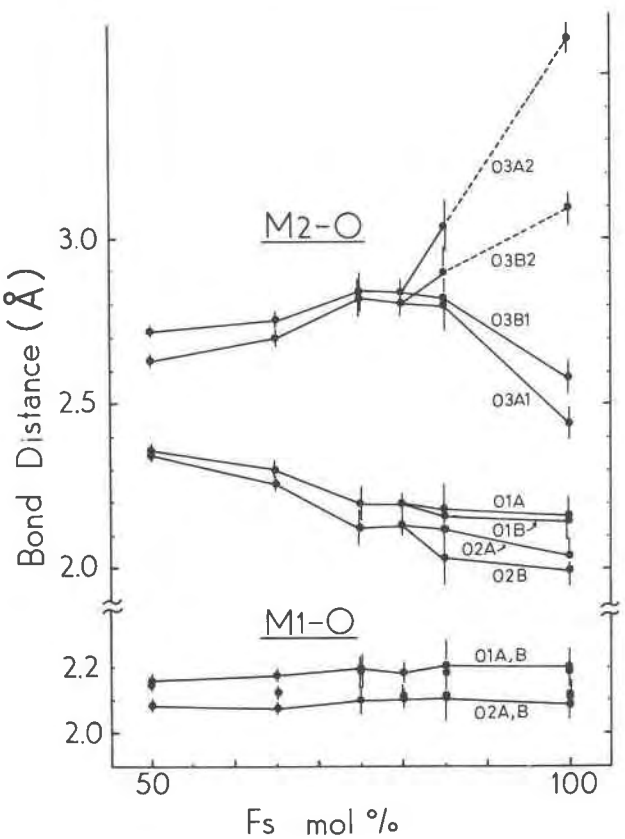

FIG. 1. Variation of $M1$–O and $M2$–O interatomic distances with ferrosilite content in Ca-Fe clinopyroxenes. Error bars represent ±1 standard deviation. Data for hedenbergite and clinoferrosilite are after Cameron *et al* (1973) and Burnham (1967), respectively. See Figure 2 for details of $M2$ coordination geometry.

(100) accompanied by relative movements of the O1 and O2 atoms toward $M2$. Rotations of the O3B1–O3B2 vector, for example, result in an increase of $M2$–O3B2 and decrease of $M2$–O3B1.

The question arises whether the structural changes described above are real changes of polyhedral geometry. If the shape of any given $M2$ coordination polyhedron is governed only by the species of atom (Ca or Fe) occupying that site (case 1), there will be only two possible types of $M2$ polyhedra in the pyroxenes studied, one found in hedenbergite and the other in clinoferrosilite, and the crystal structure of an intermediate phase obtained by X-ray diffraction would be an average of the two. In case 1, therefore, discussion of the $M2$ polyhedral geometry for intermediate compositions would have little physical meaning because the average would not represent the real structure. On the other hand, if the shape of any given $M2$ polyhedron is determined not only by the atomic species in the site but also by those in the neighboring $M2$ sites (case 2), then there are various possibilities for the $M2$ polyhedral shapes. In this case structural refinement of the X-ray data would still yield an average structure, but it would approximate the true structure more closely than in case 1.

Results of a Mössbauer study on these clinopyroxenes (Dowty and Lindsley, 1973) may help to resolve these two cases. The quadrupole splitting can be correlated with the degree of polyhedral distortion and thus it reflects primarily a short-range atomic arrangement around the *iron* atom. The change of the $M2$ quadrupole splitting (Fig. 3) indicates that the local configuration around the ferrous ion changes as the bulk chemical composition changes. Thus the $M2$ polyhedron occupied by the ferrous ion is also affected by the Fe/(Fe + Ca) ratio in the rest of the structure. Therefore, it is concluded that the $M2$ polyhedron obtained from X-ray refinement is not an artifact but represents the most probable polyhedral geometry for a given chemical composition.

Both the X-ray and the Mössbauer results indicate that a great change in the $M2$ polyhedral shape occurs at compositions between $Fs_{85}Wo_{15}$ and $Fs_{100}Wo_0$ (Fig. 3). The fact that the most rapid change occurs near the Fe-rich end of the solid solution is explained by the more severe effect expected for substitution of large Ca atoms into the small $M2$ polyhedron.

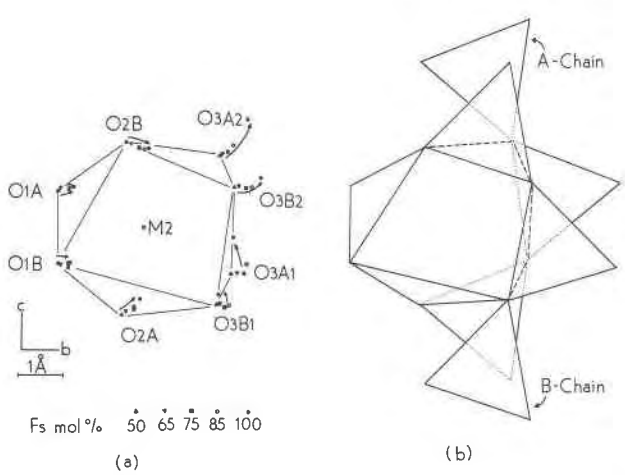

FIG. 2. (a) Variation of the oxygen positions around the $M2$ site in Ca-Fe clinopyroxenes. Arrows indicate shifts of the oxygen atoms *relative* to the $M2$ atom with Ca-Fe substitution; these may not represent actual shifts in the structure (see text, section on temperature factors, for discussion). Data for hedenbergite and clinoferrosilite are after Cameron *et al* (1973) and Burnham (1967), respectively. (b) Relation between the $M2$ site and the tetrahedral chains in $Fs_{85}Wo_{15}$. Note that positional changes of the O3 atoms shown in (a) result in rotations of the tetrahedral chains.

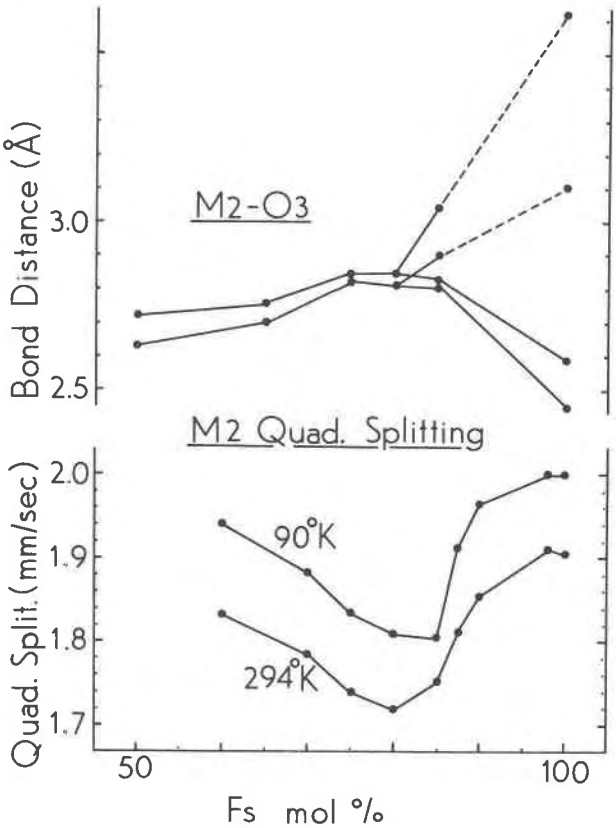

FIG. 3. Comparison of variations of the *M*2 quadrupole splitting (Dowty and Lindsley, 1973) and the *M*2–O3 interatomic distances with ferrosilite content in Ca-Fe clinopyroxenes. See Figure 1 for *M*2–O1 and *M*2–O2 distance variations. Note that both X-ray and Mössbauer studies indicate a sharp change in *M*2 polyhedral shape between the compositions $Fs_{85}Wo_{15}$ and $Fs_{100}Wo_0$.

Silicate Chains

Octahedral expansion affects the tetrahedal chains in three ways: (1) The silicate tetrahedra distort, (2) the tetrahedral chain angles change, and (3) the degree of out-of-plane tilting of the basal faces of the tetrahedra vary (Cameron *et al,* 1973). Details of these changes associated with Ca-Fe substitution are discussed below.

Tetrahedron. Interatomic distances and angles for the silicate tetrahedra are given in Table 6. The Si–O3 (bridging oxygen) bond is the longest of the Si–O bonds, and of the two nonbridging oxygens, the Si–O2 distance is shorter than the Si–O1. The angle O1–Si–O2, 114°–119°, is larger than the ideal tetrahedral angle, 109.46°.

The Si–O3 (bridging) bond distances (Fig. 4) decrease with replacement of Fe for Ca on the augite (Ca-rich) side, whereas the Si–O (nonbridging) bond distances increase. Variation on the pigeonite (Ca-poor) side, however, is not simple because there are two crystallographically distinct silicate chains. As the composition changes from $Fs_{50}Wo_{50}$ to $Fs_{75}Wo_{25}$, expansions of the Si–O1 and Si–O2 bonds are accompanied by contractions of *M*2–O1 and *M*2–O2, respectively. For the O3 atoms, contractions of the Si–O3 bonds are coupled with expansions of the *M*2–O3 bonds. The *M*1–O distances remain essentially constant with composition.

Qualitative discussions on bond distances can be developed by introducing a *bond strength,* defined by Zachariasen (1963). He assumes (1) that the bond strength is empirically related to the bond distance and (2) that the sum of bond strengths for each atom is set to its valence. Coupled changes in the Si–O and *M*2–O bond distances for the same oxygen atom are a natural consequence of the constant sum of the bond

TABLE 6. Interatomic Distances and Angles for Si Tetrahedra in Ca-Fe Clinopyroxenes

	$Fs_{65}Wo_{35}$	$Fs_{75}Wo_{25}$	$Fs_{80}Wo_{20}$	$Fs_{85}Wo_{15}$ A Chain	$Fs_{85}Wo_{15}$ B Chain
Distances (Å)					
Si-O1	1.602(2)*	1.621(6)	1.614(3)	1.616(7)	1.620(7)
-O2	1.593(2)	1.601(7)	1.596(3)	1.589(11)	1.616(8)
-O3(1)	1.672(2)	1.657(7)	1.660(3)	1.642(8)	1.677(8)
-O3(2)	1.657(2)	1.667(7)	1.647(3)	1.630(7)	1.640(6)
Mean, Nbr**	1.598	1.611	1.605	1.603	1.618
Mean, Br**	1.665	1.662	1.654	1.636	1.659
Mean of 4	1.631	1.637	1.629	1.619	1.638
Quad. Elong.***	1.0048	1.0044	1.0042	1.0016	1.0067
O1-O2	2.728(3)	2.747(7)	2.737(4)	2.694(9)	2.783(9)
O1-O3(1)	2.678(3)	2.671(8)	2.668(5)	2.643(10)	2.672(11)
O1-O3(2)	2.669(3)	2.681(9)	2.658(4)	2.630(9)	2.666(9)
O2-O3(1)	2.580(3)	2.574(9)	2.573(5)	2.601(14)	2.565(13)
O2-O3(2)	2.655(3)	2.676(10)	2.648(5)	2.636(11)	2.652(10)
O3(1)-O3(2)	2.647(1)	2.664(2)	2.659(2)	2.654(2)	2.688(3)
Angles (deg.)					
O1-Si-O2	117.2(1)	117.0(4)	117.0(2)	114.4(6)	118.7(6)
O1-Si-O3(1)	109.7(1)	109.2(3)	109.2(2)	108.4(4)	108.3(4)
O1-Si-O3(2)	109.9(1)	109.2(3)	109.2(2)	108.2(4)	109.7(4)
O2-Si-O3(1)	104.4(1)	104.4(4)	104.4(2)	107.3(5)	102.3(5)
O2-Si-O3(2)	109.5(1)	110.0(4)	109.4(2)	109.9(4)	109.1(4)
O3(1)-Si-O3(2)	105.3(1)	106.6(3)	107.1(1)	108.4(3)	108.2(3)
Ang. Var. (deg.^{2})†	20.7	18.4	17.9	6.9	28.2
O3-O3-O3††	162.5(2)	159.8(5)	159.5(3)	164.2(8)	156.0(7)
Si-O3-Si	136.5(1)	136.6(5)	136.8(2)	140.9(5)	135.5(5)
Out-of-plane tilting†††	3.7	4.5	4.7	4.2	5.8
Tetrahedral Volume (Å^3)	2.214	2.233	2.206	2.175	2.236

*Parenthesized figures represent the estimated standard deviation (esd) in terms of least units cited for the value to their immediate left, thus for 1.602(2) read 1.602 ± 0.002.

**Nbr = nonbridging oxygen atoms (O1 and O2), and
Br = bridging oxygen atom (O3).

***Tetrahedral quadratic elongation (Robinson et al., 1971) defined by $\sum_{i=1}^{4} (l_i/l_o)^2/4$, where l_o is the center-to-vertex distance for an ideal tetrahedron whose volume is equal to the observed tetrahedron.

†Tetrahedral angle variance (Robinson et al., 1971) defined by $\sum_{i=1}^{6} (\theta_i - 109.47°)^2/5$.

††Tetrahedral chain angle. All chains listed here are 0 rotation (Thompson, 1970).

†††Angle between (100) and the basal face, O2-O3-O3, of a tetrahedron.

strengths. When the strength of one bond increases, that of another must decrease to maintain the sum constant. Because only three cations are coordinated to the O2 atom, the bond strengths for Si–O2, *M*1–O2, and *M*2–O2 are larger (thus shorter in length) than any other corresponding bonds for the O1 and O3 oxygens.

Tetrahedral Chain Angle. The tetrahedral chain angle, O3–O3–O3, has been shown to vary with chemical composition, particularly with Ca content, and also with temperature (Clark *et al,* 1969; Brown *et al,* 1972; Smyth and Burnham, 1972; Cameron *et al,* 1973). Proper attention must be given, however, not only to angles but also to the rotation direction with respect to the octahedra (Thompson, 1970; Papike *et al,* 1973). Overlooking the difference in the rotation sense, the chain in augites is often compared with the *A* chain in pigeonites on the basis of the apparent similarity of the tetrahedral chain angle, which is 165° for hedenbergite (Cameron *et al,* 1973) and 167° for the *A* chain in clinoferrosilite (Burnham, 1967). The sense of rotation is, however, reversed in these chains.

The variation of the tetrahedral chain angles with composition is plotted in Figure 5. As the effective size of *M*2 decreases by substitution of Fe for Ca, the chain becomes more kinked, from 165° in $Fs_{50}Wo_{50}$ to 159° in $Fs_{80}Wo_{20}$. The relation between the *M*2 site and the tetrahedral chains can be visualized using Figure 2: a vector connecting O3*B*1 and O3*B*2 can be seen to rotate clockwise when the composition changes from $Fs_{50}Wo_{50}$ to $Fs_{80}Wo_{20}$, and this rotation results in a decrease in the O3–O3–O3 angle. As the size of *M*2 decreases further from $Fs_{80}Wo_{20}$, the chains on opposite sides of each *M*2 polyhedron become crystallographically distinct. The *B* chain becomes increasingly kinked, whereas the *A* chain becomes extended and reverses its rotation direction between $Fs_{85}Wo_{15}$ and $Fs_{100}Wo_0$. Thus in $Fs_{100}Wo_0$ the *A* chain is "S-rotated" (Thompson, 1970) and the *B* chain is "O-rotated."

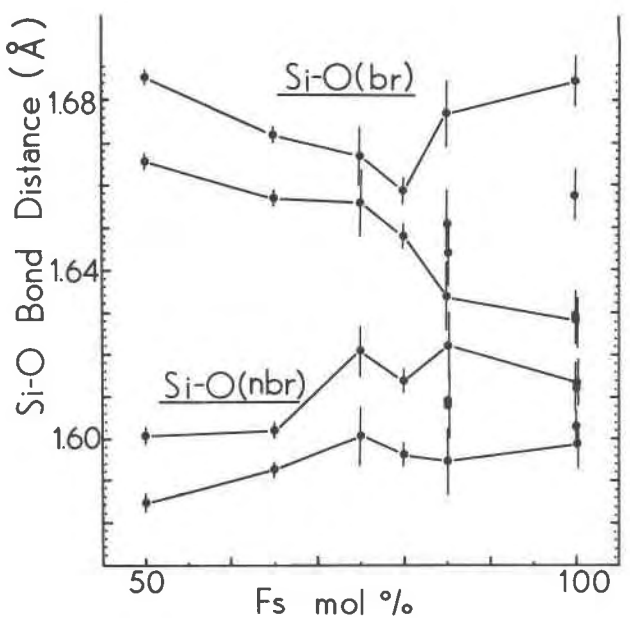

FIG. 4. Variation of Si–O interatomic distances with ferrosilite content in Ca-Fe clinopyroxenes. Error bars represent ±1 standard deviation. O(br) denotes the bridging oxygen atom, O3; O(nbr) denotes the nonbridging oxygen atoms, O1 and O2. Distances in hedenbergite and clinoferrosilite are after Cameron *et al* (1973) and Burnham (1967), respectively.

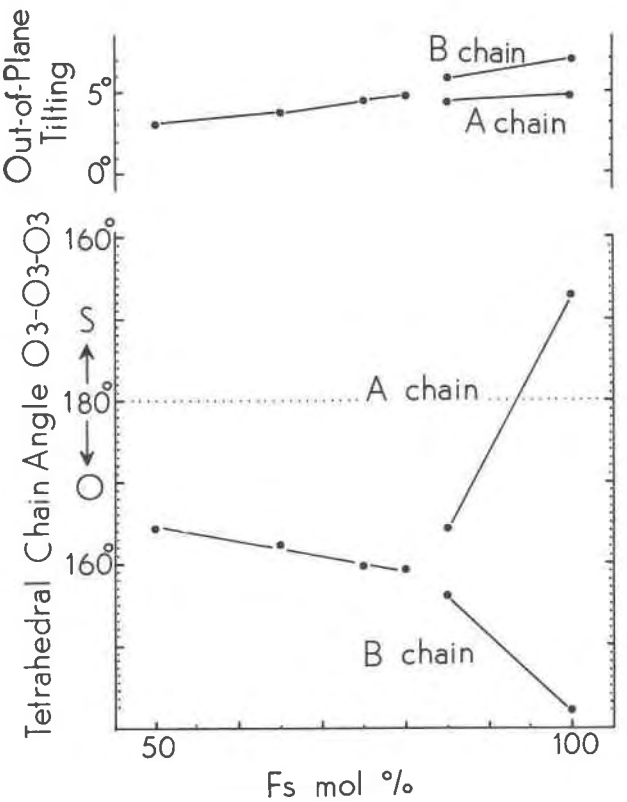

FIG. 5. Variation of the tetrahedral chain angle, O3–O3–O3, and the out-of-plane tilting of the basal triangle, defined by O2, O3, and O3, with the ferrosilite component in Ca-Fe clinopyroxenes. Angles for hedenbergite and clinoferrosilite were computed from the atomic coordinates given by Cameron *et al* (1973) and Burnham (1967), respectively. Standard errors are smaller than the radii of circles.

Out-of-Plane Tilting of the Basal Face of the Tetrahedron. The out-of-plane tilting of the basal face of the tetrahedron, which is defined as the angle between (100) and the basal face,

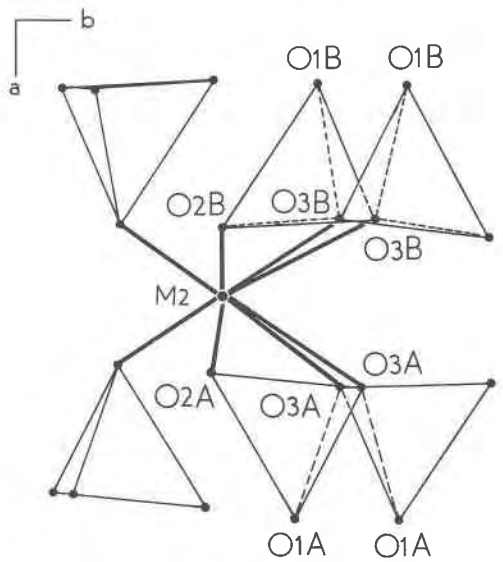

FIG. 6. A portion of the $Fs_{85}Wo_{15}$ structure showing the relation between the $M2$ site and the out-of-plane tilting of the basal face of the tetrahedron. The O2 atoms shift slightly toward $M2$ and away from the (100) plane, passing through the O3 atoms. As a result, the basal face of the tetrahedron tilts a few degrees with respect to (100). Out-of-plane tilting increases when the effective ionic size of $M2$ decreases, as would be expected from shortening of $M2$–O2 bonds.

O2–O3–O3′, of the tetrahedron, provides another measure to describe the silicate tetrahedral chain configuration. The direction of the observed tilting is such that the O1 and O2 atoms in the same tetrahedron are on opposite sides of the (100) plane containing the O3 atoms (Fig. 6). As exhibited in Figure 5 and Table 5, the out-of-plane tilting generally tends to increase when the composition changes from hedenbergite to ferrosilite. This increased tilting is a direct response of the tetrahedral chain to the changes in the $M2$ polyhedron. When the composition changes from $Fs_{50}Wo_{50}$ to $Fs_{80}Wo_{20}$ (Fig. 1), the $M2$–O2 distances decrease but $M2$–O3 distances increase. These changes in the $M2$–O distances will result in an increase in the out-of-plane tilting angle (Fig. 6). In the pigeonite region the tilting is larger for the B chain than for the A chain, reflecting the fact that $M2$–O2B < $M2$–O2A and $M2$–O3B1 > $M2$–O3A1 (Fig. 1).

There is a correlation between the tilting and the tetrahedral B chain angle (Fig. 5)—the more kinked the chain angle, the greater the out-of-plane tilting. This relationship may be explained by simple geometrical arguments. The kinking of the chain results in an increase in the offset of O3 atom pairs parallel to b (Fig. 2b). However, these changes have very little effect on the O1–O1 distance, which varies only from 3.088 Å in $Fs_{50}Wo_{50}$ to 3.040 Å in $Fs_{100}Wo_0$ as the chain angle decreases from 164.5° to 142°; therefore, the relative position of O1 is very nearly fixed. The only means of kinking the chain without moving O1 results in the movement of the O2 atom in such a manner that the out-of-plane tilting increases (Fig. 6).

Temperature Factors

The variation of isotropic temperature factors with composition (Fig. 7) falls into two groups: one ($M2$, O2, and O3) has a marked peak in the middle of the solid solution, whereas the other ($M1$, Si, and O1) is relatively flat. These differences in behavior can be explained by the effects of positional disorder due to multiple occupancy of the $M2$ site. Because the ionic radii of the Ca and Fe atoms are considerably

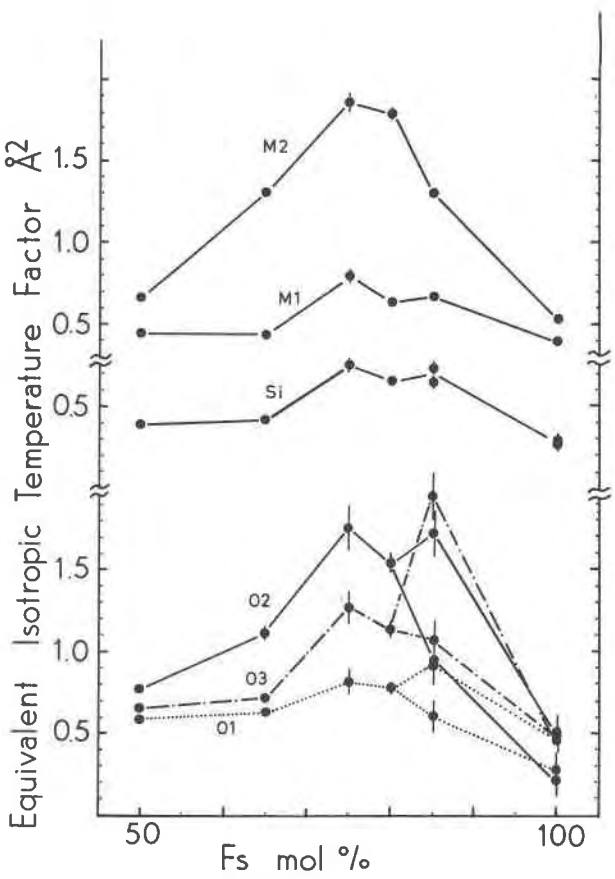

FIG. 7. Variation of equivalent isotropic temperature factors with ferrosilite content in Ca-Fe clinopyroxenes. Error bars represent ±1 standard deviation (if not shown, the standard deviation is smaller than the radii of circles). Data for hedenbergite and clinoferrosilite are after Cameron *et al* (1973) and Burnham (1967), respectively.

different, one might expect a positional fluctuation, which results from variation of the atomic positions (in terms of fractional coordinates of the unit-cell translations) from one unit cell to another. The effects of positional disorder may be significant, especially for the multiple occupancy sites.

In the clinopyroxenes under study, the *M*2 site shows its largest apparent temperature factor in the middle of the solid solution (Fig. 7), as is expected from its multiple occupancy by Ca and Fe atoms. The O2 and O3 atoms also exhibit large apparent temperature factors for intermediate compositions. This effect can be related to disorder of the tetrahedral chain rotation, as will be discussed below. In contrast *M*1 and Si, which are not directly linked to *M*2, show less significant effects of positional disorder. Interestingly, the positional disorder of the apical oxygen O1, although it is coordinated to *M*2, is the smallest among the oxygen atoms, indicating that the position of O1 is relatively well localized in the unit cell.

Some of the thermal vibration ellipsoids given in Table 7 show abnormally large anisotropy, which may be explained by positional disorder. The apparent thermal vibration ellipsoids for the atoms in the *M*2 polyhedron are shown in Figure 8. *M*2, for example, has the longest ellipsoid axis parallel to the *b* axis, except in hedenbergite, in which the longest axis is normal to the *b* axis. The thermal vibration ellipsoid in hedenbergite presumably represents

TABLE 7. Magnitudes and Orientations of the Principal Axes of Thermal Vibration Ellipsoids in Ca-Fe Clinopyroxenes

	Ellipsoid axis, r_i	r.m.s. amplitude (Å)	Angle (deg.) of r_i with a	b	c	r.m.s. amplitude (Å)	Angle (deg.) of r_i with a	b	c	r.m.s. amplitude (Å)	Angle (deg.) of r_i with a	b	c
		M1				M2				Si			
$Fs_{65}Wo_{35}$	1	0.066(2)*	90	0	90	0.078(2)	76(2)	90	30(2)	0.058(3)	114(7)	62(8)	30(6)
	2	0.069(2)	78(4)	90	177(4)	0.113(1)	166(2)	90	60(2)	0.070(3)	129(8)	140(8)	73(8)
	3	0.087(1)	12(4)	90	93(4)	0.175(1)	90	0	90	0.086(2)	49(5)	116(5)	66(4)
$Fs_{75}Wo_{25}$	1	0.092(5)	8(12)	90	98(12)	0.092(6)	49(5)	90	58(5)	0.083(6)	16(43)	76(48)	112(9)
	2	0.101(4)	90	0	90	0.142(5)	41(5)	90	148(5)	0.090(6)	76(47)	166(48)	96(22)
	3	0.109(5)	98(12)	90	8(12)	0.204(4)	90	0	90	0.116(5)	84(7)	90(14)	23(7)
$Fs_{80}Wo_{20}$	1	0.073(2)	139(18)	90	115(18)	0.100(2)	170(6)	90	83(6)	0.057(3)	139(9)	83(6)	114(8)
	2	0.080(2)	90	0	90	0.118(2)	109(6)	90	145(6)	0.080(3)	94(6)	161(3)	106(5)
	3	0.112(2)	109(5)	90	3(5)	0.209(2)	90	0	90	0.122(2)	110(5)	106(3)	17(3)
										SiA			
$Fs_{85}Wo_{15}$	1	0.086(4)	23(15)	112(24)	114(30)	0.084(2)	50(3)	92(2)	58(3)	0.070(7)	14(8)	103(10)	101(9)
	2	0.091(4)	87(34)	63(17)	149(26)	0.118(2)	41(3)	85(2)	147(3)	0.096(7)	92(12)	124(13)	141(12)
	3	0.099(5)	67(12)	36(13)	72(18)	0.185(2)	93(2)	5(2)	85(2)	0.117(6)	104(7)	143(12)	53(12)
										SiB			
										0.063(10)	57(11)	34(10)	96(13)
										0.087(6)	52(13)	111(13)	149(10)
										0.111(7)	56(8)	115(8)	59(10)
		O1				O2				O3			
$Fs_{65}Wo_{35}$	1	0.083(6)	87(102)**	133(154)	46(186)	0.080(6)	71(8)	25(3)	79(9)	0.069(7)	99(12)	66(5)	24(5)
	2	0.084(6)	58(18)	127(160)	136(186)	0.105(5)	41(6)	94(9)	146(5)	0.090(5)	169(11)	89(8)	85(12)
	3	0.100(4)	33(14)	65(13)	84(13)	0.156(4)	55(4)	115(3)	58(4)	0.117(5)	85(8)	24(5)	114(5)
$Fs_{75}Wo_{25}$	1	0.061(27)	127(21)	48(14)	53(10)	0.092(17)	50(35)	40(35)	101(14)	0.086(16)	27(26)	112(12)	119(26)
	2	0.098(17)	143(21)	120(20)	95(17)	0.110(15)	139(35)	50(35)	70(9)	0.107(13)	112(29)	108(15)	137(23)
	3	0.135(15)	90(15)	124(11)	37(9)	0.215(12)	83(5)	95(5)	24(6)	0.171(11)	75(7)	29(8)	118(8)
$Fs_{80}Wo_{20}$	1	0.076(7)	115(17)	99(13)	108(16)	0.072(8)	131(29)	53(32)	104(11)	0.065(9)	134(13)	101(5)	118(12)
	2	0.101(6)	80(15)	167(18)	85(19)	0.094(7)	119(24)	125(14)	120(16)	0.111(6)	56(13)	126(6)	136(9)
	3	0.117(5)	96(11)	88(21)	10(12)	0.210(5)	115(7)	111(3)	24(4)	0.164(5)	90(3)	147(4)	59(4)
$Fs_{85}Wo_{15}$ A chain	1	0.054(22)	52(13)	92(32)	56(13)	0.110(13)	146(15)	74(28)	45(9)	0.032(45)	35(12)	104(7)	76(9)
	2	0.093(17)	99(49)	169(56)	82(48)	0.133(15)	105(25)	164(28)	79(21)	0.108(13)	56(12)	59(5)	142(6)
	3	0.106(12)	140(19)	79(56)	35(19)	0.187(13)	61(7)	92(12)	47(7)	0.248(11)	96(3)	35(3)	55(3)
	1	0.084(15)	153(24)	78(22)	49(18)	--***	51(15)	43(12)	87(10)	0.041(30)	143(9)	104(6)	40(8)
B chain	2	0.113(20)	116(25)	126(43)	120(35)	0.106(21)	40(15)	124(13)	120(10)	0.129(14)	125(10)	86(19)	127(10)
	3	0.128(17)	84(26)	141(41)	56(28)	0.166(11)	86(8)	112(7)	30(9)	0.157(12)	99(13)	15(8)	76(13)

*Parenthesized figures represent the estimated standard deviation (esd) in terms of least units cited for the value to their immediate left, thus for 0.066(2) read 0.066 ± 0.002.
**Orientation of axis is indeterminate because the ellipsoid is essentially uniaxial.
***The corresponding eigen value is close to zero but negative.

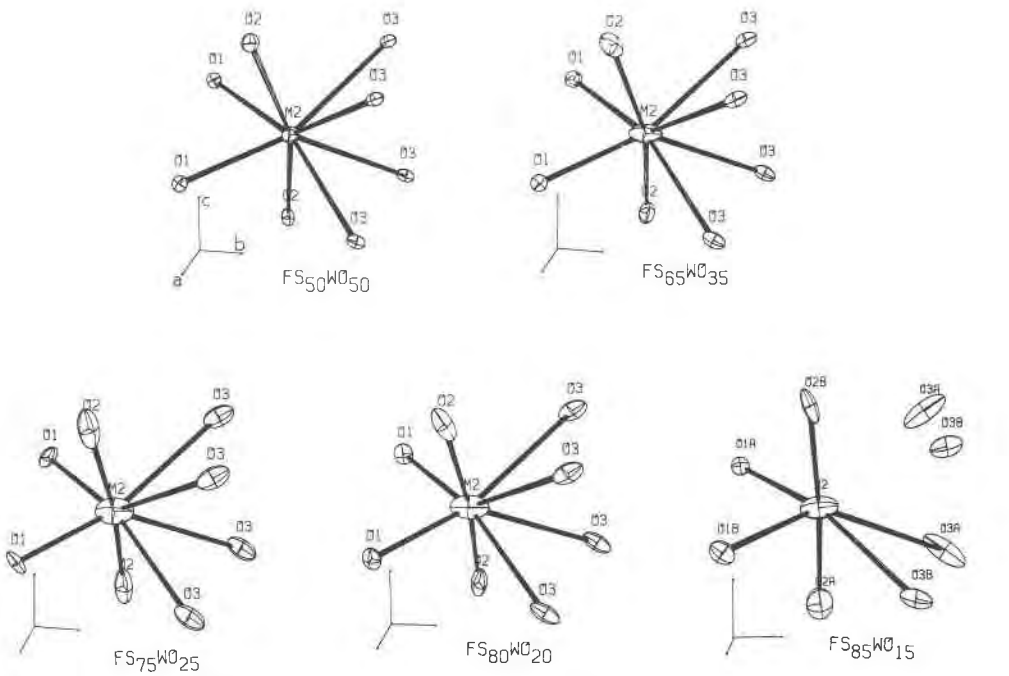

FIG. 8. Apparent thermal vibration ellipsoids for atoms in the *M*2 polyhedron in Ca-Fe clinopyroxenes. The ellipsoids represent 70 percent probability surfaces (1.92 times the r.m.s. amplitude). Ellipsoids for hedenbergite were calculated from data given by Veblen (1969). For the O2*B* site in $Fs_{85}Wo_{15}$, β_{13} is decreased by 2 standard deviations to obtain a positive definite tensor. Drawing produced by ORTEP (Johnson, 1965).

primarily intrinsic vibrations, whereas those in intermediate compositions include significant effects of positional disorder. As for the *M*2 displacement, this study suggests the same interpretation reached by Takeda (1972). Since O1 shows relatively small changes in ellipsoid shape throughout the solid solution, it seems reasonable to conclude that as the composition becomes more iron-rich, the mean position of *M*2 shifts toward O1 rather than the other way.

In intermediate compositions the longest ellipsoid axis for the O2 atom tends to orient parallel to the bond direction of *M*2–O2 (Fig. 9a). Since *M*2–O2 is the shortest bond in the *M*2 polyhedron, the multiple occupancy of the Ca and Fe atoms in *M*2 may produce significant disorder of O2 along the bond direction.

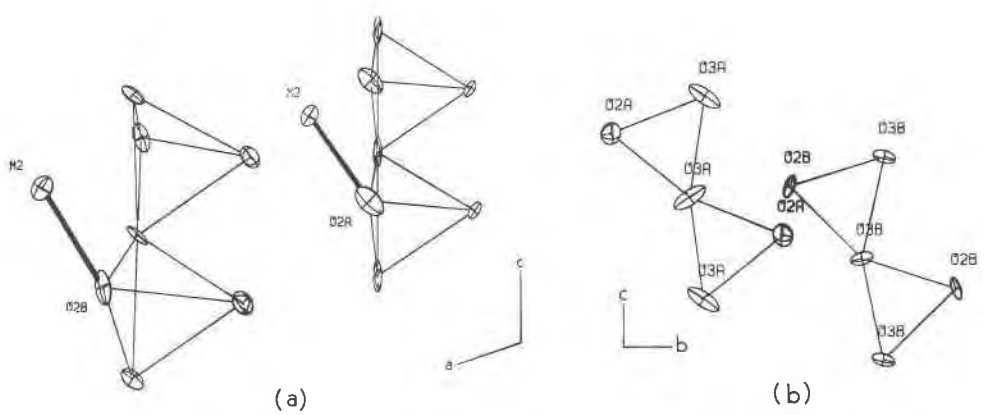

FIG. 9. Explanation of the abnormally large apparent thermal vibration ellipsoids for O2 and O3 atoms in $Fs_{85}Wo_{15}$. See text. Ellipsoids shown are 70 percent probability surfaces (1.92 times the r.m.s. amplitude). For the O2*B* atom, β_{13} is decreased by 2 standard deviations to obtain a positive definite tensor. Drawing produced by ORTEP (Johnson, 1965).

The large apparent thermal vibration ellipsoid for the O3 atoms in the intermediate compositions can be interpreted as positional disorder associated with tetrahedral chain rotation (Fig. 9b). As previously shown (Fig. 2) the change in size of the $M2$ cation causes a rotation of the tetrahedral chains. The rotation angle of the individual chains may be slightly different from the average chain angle, and the resulting positional fluctuation will appear as large apparent vibrations of O3 in (100), the approximate plane of the rotation, and along a bisecting direction of the basal faces of the two tetrahedra bridged by O3. O1 and Si, however, are close to the rotation axis and thus are not affected by this rotation.

Conclusions

As composition changes on the hedenbergite-ferrosilite join, the polyhedral volume and bond distances of the $M1$ site do not change appreciably, except for a slight distortion of the polyhedron. Such lack of change in $M1$ confirms that few, if any, Ca atoms can occupy $M1$ sites in the Ca-Fe clinopyroxenes studied.

In the $M2$ coordination polyhedron the $M2$–O1 and $M2$–O2 distances and the polyhedral volume decrease when the composition changes from hedenbergite to ferrosilite. The $M2$–O3 distances exhibit a sharp change between the compositions $Fs_{85}Wo_{15}$ and $Fs_{100}Wo_0$.

The decrease in the average size of the $M2$ atom causes kinking of the tetrahedral B chain. Extension and reversal of rotation sense of the A chain occur between the compositions $Fs_{85}Wo_{15}$ and $Fs_{100}Wo_0$. The decrease in $M2$ cation size causes an increase in the out-of-plane tilting of the basal face of the tetrahedron.

The large temperature factors found for the $M2$, O2, and O3 atoms in intermediate compositions of the Ca-Fe clinopyroxenes can be explained by the effect of atomic positional disorder due to multiple occupancy in $M2$.

Together with the crystal structures of the end-member clinopyroxenes at high temperatures (Cameron *et al,* 1973), the results of the present study could provide a basis for future studies of the crystal structures of intermediate clinopyroxenes at high temperature. These studies, which will undoubtedly have mineralogical significance for a better understanding of crystallization and exsolution in natural pyroxenes, are also necessary for relating the crystal structures to the experimentally determined phase diagram.

Acknowledgments

We thank Dr. D. H. Lindsley for supplying the synthetic pyroxene crystals, and Drs. H. S. Yoder, Jr., G. E. Brown, C. T. Prewitt, and S. Sueno for their many helpful comments and suggestions on the manuscript. The present study is based partly on the first author's Ph.D. dissertation (Ohashi, 1973), accepted by the Department of Geological Sciences, Harvard University. That part of the study was supported by the National Science Foundation grant GA-12852 to C.W.B. The remainder of the work was performed at the Geophysical Laboratory, Carnegie Institution of Washington. Thanks are due Miss D. M. Thomas for editing and typing the manuscript.

References

Bowen, N. L., J. F. Schairer, and E. Posnjak (1933) The system CaO–FeO–SiO_2. *Am. J. Sci.* **26,** 193–284.

Brown, G. E., C. T. Prewitt, J. J. Papike, and S. Sueno (1972) A comparison of the structures of low and high pigeonite. *J. Geophys. Res.* **77,** 5778–5789.

Burnham, C. W. (1962) Lattice constant refinement. *Carnegie Inst. Wash. Year Book,* **61,** 132–135.

——— (1966) Computation of absorption correction and the significance of end effect. *Am. Mineral.* **51,** 159–167.

——— (1967) Ferrosilite. *Carnegie Inst. Wash. Year Book,* **65,** 285–290.

———, J. R. Clark, J. J. Papike, and C. T. Prewitt (1967) A proposed crystallographic nomenclature for clinopyroxene structures. *Z. Kristallogr.* **125,** 109–119.

Cameron, M., S. Sueno, C. T. Prewitt, and J. J. Papike (1973) High-temperature crystal chemistry of acmite, diopside, hedenbergite, jadeite, spodumene, and ureyite. *Am. Mineral.* **58,** 594–618.

Clark, J. R., D. E. Appleman, and J. J. Papike (1969) Crystal-chemical characterization of clinopyroxenes based on eight new structure refinements. *Mineral. Soc. Am. Spec. Pap.* **2,** 31–50.

Cromer, D. T. (1965) Anomalous dispersion corrections computed from self-consistent field relativistic Dirac-Slater wave functions. *Acta Crystallogr.* **18,** 17–23.

———, and J. B. Mann (1968) X-ray scattering factors computed from numerical Hartree-Fock wave functions. *Acta Crystallogr.* **24,** 321–324.

Dowty, E., and D. H. Lindsley (1973) Mössbauer spectra of synthetic hedenbergite-ferrosilite pyroxenes. *Am. Mineral.* **58,** 850–868.

Gabe, E. J., G. E. Alexander, and R. H. Goodman (1970) The Mines Branch on-line single-crystal diffractometer. *Mineral Sci. Div., Dep. Energy, Mines Resources, Canada, Internal Rep.* **MS71-54.**

Güven, N. (1969) Nature of the coordination polyhedra around $M2$ cations in pigeonite. *Contrib. Mineral. Petrol.* **24,** 268–274.

Hamilton, W. C. (1959) On the isotropic temperature factor equivalent to a given anisotropic temperature factor. *Acta Crystallogr.* **12,** 609–610.

Johnson, C. K. (1965) Ortep, a Fortran thermal ellipsoid plot program for crystal structure illustrations. *U.S. Nat. Tech. Inform. Serv.* **ORNL-3794.**

Lindsley, D. H., and J. L. Munoz (1969) Subsolidus relations along the join hedenbergite–ferrosilite. *Am. J. Sci.* **267A,** 295–324.

Morimoto, N., D. Appleman, and H. T. Evans (1960) The

crystal structures of clinoenstatite and pigeonite. *Z. Kristallogr.* **114,** 120–147.

———, AND N. GÜVEN (1970) Refinement of the crystal structure of pigeonite. *Am. Mineral.* **55,** 1195–1209.

OHASHI, Y. (1973) *High Temperature Structural Crystallography of Synthetic Clinopyroxene,* (Ca,Fe)SiO_3. Ph.D. Thesis, Harvard University.

———, AND C. W. BURNHAM (1973) Clinopyroxene lattice deformations: the roles of chemical substitution and temperature. *Am. Mineral.* **58,** 843–849.

PAPIKE, J. J., C. T. PREWITT, S. SUENO, AND M. CAMERON (1973) Pyroxenes: comparisons of real and ideal structural topologies. *Z. Kristallogr.* **138,** 254–273.

ROBINSON, K., G. V. GIBBS, AND P. H. RIBBE (1971) Quadratic elongation: a quantitative measure of distortion in coordination polyhedra. *Science,* **172,** 567–570.

SMYTH, J. R., AND C. W. BURNHAM (1972) The crystal structures of high and low clinohypersthene. *Earth Planet. Sci. Lett.* **14,** 183–189.

TAKEDA, H. (1972) The crystallography of some aluminous orthopyroxenes of high pressure origin. *J. Geophys. Res.* **77,** 5798–5811.

THOMPSON, J. B., JR. (1970) Geometrical possibilities for amphibole structures. *Am. Mineral.* **55,** 292–293.

VEBLEN, D. R. (1969) *The Crystal Structures of Hedenbergite and Ferrosilite.* A. B. Thesis, Harvard University.

ZACHARIASEN, W. H. (1963) The crystal structure of monoclinic metaboric acid. *Acta Crystallogr.* **16,** 385–389.

——— (1968) Experimental tests of the general formula for the integrated intensity of a real crystal. *Acta Crystallogr.* **A24,** 212–216.

Manuscript received, September 16, 1974; accepted for publication, December 19, 1974.